Short term reliability and robustness of ultra-thin barrier, 110 nrn-gate AlN/GaN HEMTs

Zhan Gao, Matteo Meneghini, Kathia Harrouche, Riad Kabouche, Francesca Chiocchetta, Etienne Okada, Fabiana Rampazzo, Carlo de Santi, F Medjdoub, Gaudenzio Meneghesso, et al.

Short Term Reliability and Robustness of ultra-thin barrier, 110 nm-gate AlN/GaN HEMTs

Zhan. Gao[1], Matteo. Meneghini[1], Kathia Harrouche[2], Riad Kabouche[2], Francesca Chiocchetta[1], Etienne Okada[2], Fabiana. Rampazzo[1], Carlo. De Santi[1], Farid Medjdoub[2], Gaudenzio. Meneghesso[1], Enrico. Zanoni[1]
[1]Dipartimento di Ingegneria dell'Informazione, Università di Padova, Via Gradenigo 6/A, 35131 Padova
[2]CNRS-IEMN, Institut d'Electronique, de Microélectronique et de Nanotechnologie, 59652 Villeneuve-d'Ascq, France
Email :gaozhan.veronica@gmail.com

***Abstract*—Short-term reliability and robustness of 110 nm AlN/GaN HEMTs has been evaluated by means off-state, semi-on state and on-state step stress tests on devices having different gate-drain distance, L_{GD}. While breakdown voltages and critical voltages scale almost linearly with L_{GD}, failure mode remains almost unchanged in the nine device groups, and consists in an increase of gate leakage, accompanied by a positive shift of threshold voltage. In off-state, electroluminescence images detect the presence of localized leakage paths which may correspond to dislocations and act as preferential paths for electron trapping. Degradation is therefore preliminary attributed to hot-electron trapping, enhanced by electric fields.**

Keywords—AlN/GaN HEMTs, reliability, stress, breakdown mechanism, electric field, radio frequency

I. INTRODUCTION

GaN-based High Electron Mobility Transistors (HEMTs) have drawn great attention due to their potential for high temperature, high frequency and high power applications to radar amplifiers or modern telecommunication systems as 5G [1]. In order to achieve power density and power added effciency at high frequency, up to Q-band, one of the most usual approaches is to scale the gate length of the devices [2], but this would lead to short channel effect. Therefore, it is necessary to optimize the epilayer design and the device layout, and reduce the gate to channel distance [3]. Recently, AlN/GaN heterostructures have been proven to be able to reach a maximum current of 2.3 A/mm and peak transconductance of 480 mS/mm [4], and state-of-the-art PAE over > 65% at 40 GHz [5], by adopting an ultra-thin (3-4 nm) AlN barrier. Good stability and robustness have been achieved by AlN/GaN/AlGaN HEMTs for Ka band operation during constant voltage stress tests [6]. Reliability of AlN/GaN HEMTs with 4 nm AlN barrier during constant voltage stress has been also studied at room temperature and high temperature [7], [8]. However, available data on the reliability and robustness of AlN/GaN HEMTs are still scarce. Effective on-wafer evaluation methods are needed during device development in order to provide a fast feedback on the different technological options.

In this work, we focus on the short-term reliability of a new generation of 110 nm-gate AlN/GaN HEMTs with ultra-scaled 3 nm AlN barrier, grown on SiC substrates. We studied parametric degradation and breakdown effects during V_{DS} step stress tests at (i) off-state (V_{GS} = -5 V), (ii) semi-on state (V_{GS} = -1 V), and (iii) on-state (V_{GS} = 0 V) and during a constant voltage stress at off state (V_{GS} = -5 V, V_{DS} = 40 V). Devices with different gate-drain distance (L_{GD}) were compared. Excellent device robustness is demonstrated for these short channel, ultra-thin barrier devices. Insight in device behavior under overstress is provided by electroluminescence imaging. Experimental details of the fabricated devices and the characterization methods are described in Section II. The comparison among devices with different L_{GD} during stress and the discussion on the degradation mechanism is shown in Section III, comments on the device breakdown voltages are at the end of that section.

II. EXPERIMENTAL DETAILS

Tested structures were fabricated on AlN/GaN heterostructures grown on SiC wafers. The thickness of the AlN layer is 3 nm, the thickness of GaN channel is 100 nm, grown by MOCVD on top of a carbon doped GaN buffer. A 10 nm in-situ SiN layer was grown to protect the surface and reduce surface trapping. Further experimental details can be found in [5]. The devices under test are two-fingers devices with gate length (L_G) of 0.11 µm, gate width (W_G) of 2×50 µm; gate-drain distances (L_{GD}) are designed to be 0.5 µm, 1.5 µm and 2.5 µm. A maximum current of 1.2 A/mm and a maximum transconductance of 400 mS/mm can be achieved. Cut off frequency (F_T) and maximum oscillation frequency (F_{max}) are respectively 63 GHz and 300 GHz, and can be achieved at V_{DS} = 20V. A thorough DC and RF characterization is discussed in [5].

In this work, drain step stress tests at off state (V_{GS} = -5 V), semi-on state (V_{GS} = -1 V) and on-state (V_{GS} = 0 V) were conducted on the devices with different L_{GD}. During stress, drain voltage was increased from 0 V to 200 V or up to catastrophic breakdown in 5 V steps, each two minutes long. During each stress step, drain and gate currents as well as EL intensity were monitored. After each stress step, the devices were kept unbiased for 5 minutes, and a standard DC characterization together was taken afterwards.

After step stress, a constant voltage stress at off-state (V_{GS} = -5 V, and V_{DS} = 40 V) was taken on the devices, in order to evaluate the devices reliability on a short time scale. DC characteristics degradation after the 24 hours' stress among devices with different L_{GD} was summarized and compared.

III. RESUTLS

A. Off-state drain step stress

Device drain current recorded during off-state stress (V_G = -5 V) is shown in Fig. 1Fig. 1(a) for the different L_{GD}: 0.5 µm, 1.5 µm and 2.5 µm. Device with L_{GD} = 2.5 µm didn't show catastrophic failure up to 200 V, while L_{GD} = 0.5 µm and 1.5 µm devices suffered destructive breakdown at 70 V and 185 V, respectively. If one adopts a failure criteria corresponding to a drain leakage current density of 1 mA/mm, the following failure voltages are obtained, respectively for L_{GD} = 0.5 µm, 1.5 µm and 2.5 µm devices: 45 V, 60 V and 70 V. The increase in leakage current is usually caused by the generation of preferential leakage current conduction paths.

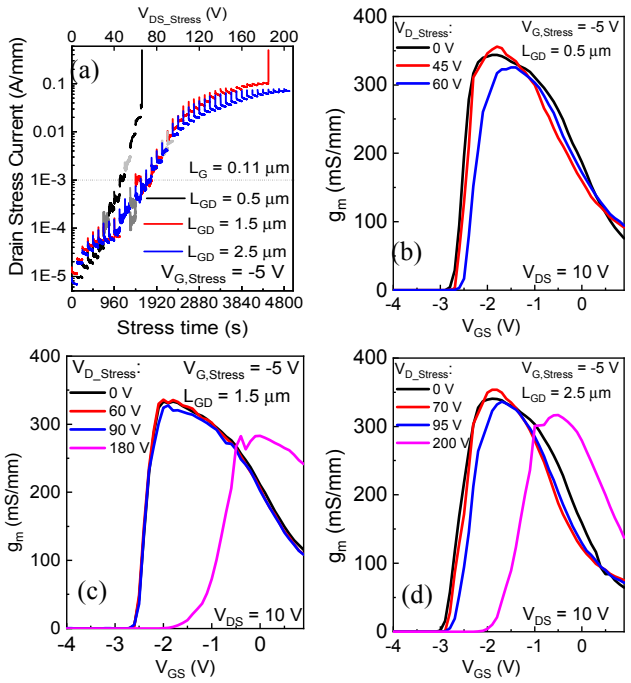

Fig. 1 (a) Drain current monitored during off-state stress and g_m-V_G curves during stress (b) L_{GD} = 0.5 µm (c) 1.5 µm and (d) 2.5 µm devices.

As the step stress proceeds, a positive threshold voltage shift occurs, in the L_{GD} = 1.5 µm device, V_{th} shift reaches approximately 1.5 V, at the same time transconductance g_m shows a decrease of 16% at stress step of 180 V. It should be noted, however, that V_{TH} shift is negligible and that no degradation of I_{Dsat} or g_m occurs until the stress voltage reaches 50 V, 85 V and 90 V, for L_{GD} = 0.5 µm, 1.5 µm and 2.5 µm devices, respectively.

The g_m-V_G curves at V_D = 10 V of the devices after the critical stress steps are shown in Fig. 1(b)-(d). Maximum drain current (I_{DSS}), ON resistance (R_{ON}) and threshold voltage (V_{TH}) evolution during stress are shown in Fig. 2. It is worth noticing that in L_{GD} = 0.5 µm devices there is no significant parametric degradation until sudden breakdown, when the drain stress voltage is over 65 V. I_{DSS} decrease and R_{ON} increase started from 85 V and 90 V, for L_{GD} = 1.5 µm and 2.5 µm devices, respectively. The I_{DSS} decrease and V_{TH} shift can be explained by trapping effects under the gate, possibly under the channel or in the buffer.

Electroluminescence images of the L_{GD} = 1.5 µm device taken before stress and after stress at (V_G = -5 V, V_D = 60 V) are shown in Fig. 3. Before stress, there is no hot spots along the finger, after 2 minutes' stress at 60 V, EL image showed leakage points along the gate finger, thus demonstrating the generation of localized leakage paths

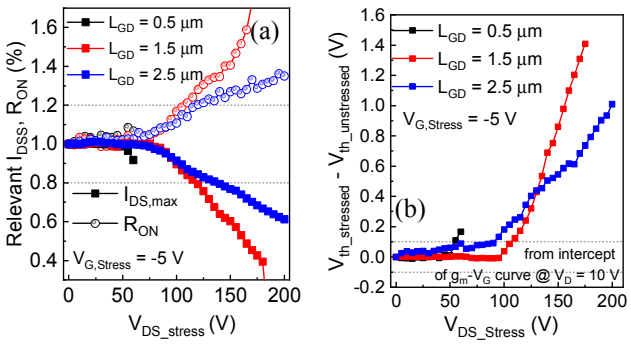

Fig. 2 (a) I_{DSS}, R_{ON} and (b) V_{TH} shift during off-state stress at $V_{G,Stress}$ = -5 V.

during stress, possibly in correspondence to defects which may also act as trapping centers.

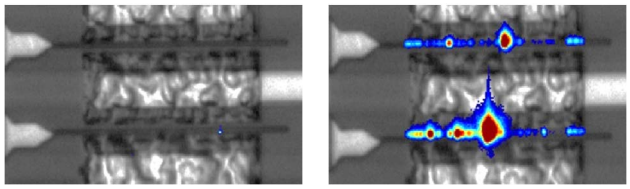

Fig. 3 Exemplary emission images (15 s emission) of the L_{GD} = 1.5 µm device (a) before stress at (V_G = -5 V, V_D = 0 V), and (b) during stress at (V_G = -5 V, V_D = 60 V).

B. Semi-on state drain step stress

Drain and gate currents of the devices with different L_{GD} recorded during semi on-state stress (V_G = -1 V) are shown in Fig. 4. Devices with 0.5 µm, 1.5 µm and 2.5 µm L_{GD} showed catastrophic failure at 50 V, 95 V and 110 V, respectively. Channel current decreases during the step stress tests, possibly due to the combined effect of device self-heating effects and electron trapping. The gate leakage current reached 1 mA/mm at stress voltages of 35 V, 65 V and 100 V, for 0.5 µm, 1.5 µm and 2.5 µm devices, respectively.

The transconductance curves of the devices at V_D = 10 V after some stress steps are shown in Fig. 4 (b)-(d). Different from what was observed during off-state stress, I_{DSS} decreased gradually, R_{ON} increased gradually, and V_{TH} showed gradual positive shift with increasing stress voltage in all devices, regardless of L_{GD}, as shown in Fig. 5. And the L_{GD} = 2.5 µm device showed the largest maximum transconductance decrease at the step before breakdown,

No leakage current increase was observed until the stress voltage exceeds 25 V, 35 V and 35 V for 0.5 µm, 1.5 µm and 2.5 µm devices, respectively, in agreement with the gate leakage current change observed during stress.

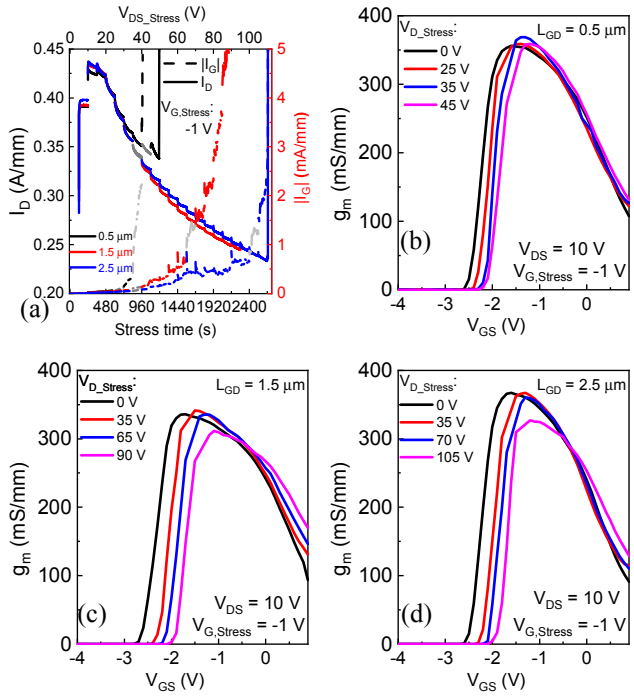

Fig. 4 (a) Drain current monitored during semi on-state stress and (b) g_m-V_G curves during stress (b) 0.5 µm (c) 1.5 µm and (d) 2.5 µm devices.

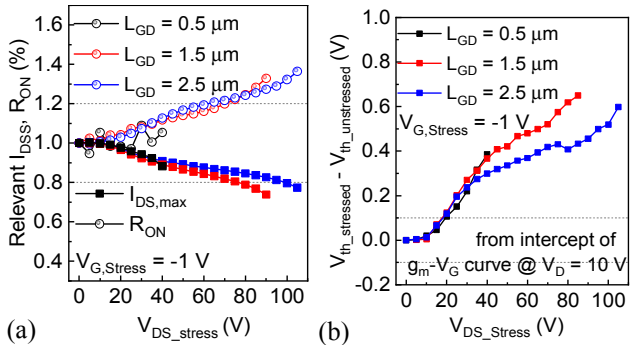

Fig. 5 (a) I_{DSS}, R_{ON} and (b) V_{TH} shift during off-state stress at $V_{G,Stress}$ = -1 V.

The EL images of the L_{GD} = 1.5 µm device taken during stress at stress (V_D = 20 V) and after stress at (V_D = 40 V) are shown in Fig. 6. An even EL intensity distribution is observed along gate fingers during tests, as shown in Fig. 6(a). At higher drain voltages emission mostly takes place at finger extremes, as carrier transport is worsened by device self-heating in the central part of the device.

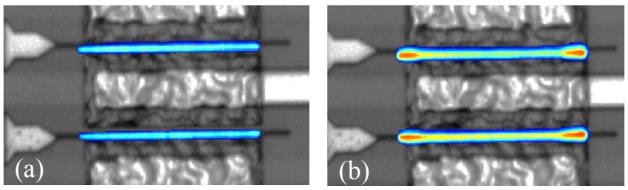

Fig. 6 Exemplary emission images (5 s) of the L_{GD} = 1.5 µm device (a) during stress at (V_G = -1 V, V_D = 20 V) and (b) (V_G = -1 V, V_D = 40 V).

C. *On-state drain step stress*

Drain and gate current of the devices recorded during on-state stress are shown in Fig. 7 (a). Despite the very large power density (15 W/mm ∽ 30 W/mm), devices with 0.5 µm, 1.5 µm and 2.5 µm of L_{GD} did not fail up to burnout occurring at 30 V, 55 V and 65 V, respectively. The failure mechanism is most possibly due to thermal effect caused by device self-heating.

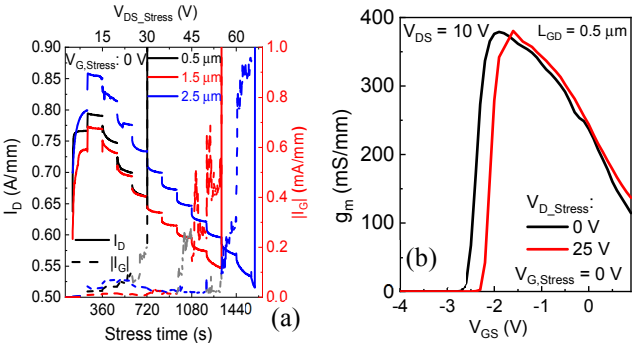

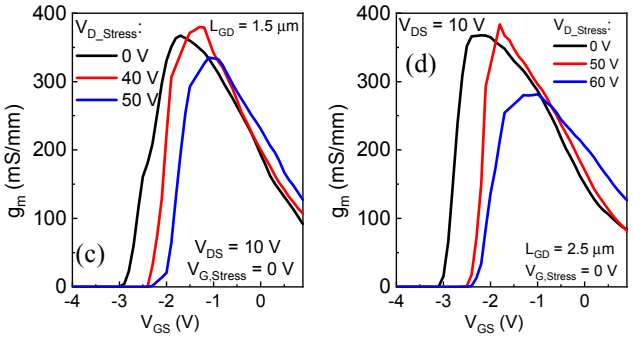

Fig. 7 (a) Drain current monitored during semi on-state stress, g_m-V_G curves during stress (b) 0.5 µm (c) 1.5 µm and (d) 2.5 µm devices.

The g_m-V_G curves of the devices at V_D = 10 V after several stress steps are shown in Fig. 7(b)-(d). Similar to the semi-on state stress, $g_{m,max}$ decrease occurred at the last stress step before breakdown, and the devices with the 2.5 µm L_{GD} have most $g_{m,max}$ degradation.

V_{TH} shifts positively with increasing stress voltage, with comparable shift in devices with different L_{GD},, possibly due to traps under the gate in the buffer or at gate edges, whose occupation and effect does not depend on by gate-drain distance, as shown in Fig. 8.

Leakage current increase can be observed, at 25 V, 40 V and 50 V for 0.5 µm, 1.5 µm and 2.5 µm devices, consistent with the gate leakage current increase monitored during stress.

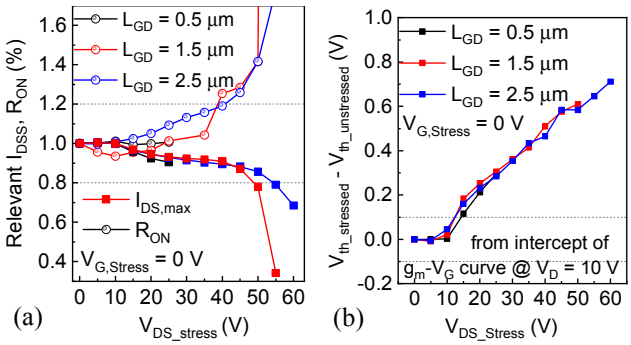

Fig. 8 (a) I_{DSS}, R_{ON} and (b) V_{TH} shift during off-state stress at $V_{G,Stress}$ = 0 V.

Fig. 9 shows breakdown voltages V_{BR} and critical voltage V_{CRI} (The voltage where leakage current exceeds 1 mA/mm) of the AlN/GaN HEMTs with difference L_{GD}. DC short-term safe operating area for the three different gate-drain spacings are also shown. It should be noted that, despite the thin barrier layer (3 nm AlN) and short channel length (110 nm), devices with the shortest L_{GD} reach off-state V_{BR} = 70 V, V_{CRI} = 55 V (50 V and 35 V in semi-on, on state) and can withstand a DC dissipated power as high as P_D = 15 W/mm in on-state.

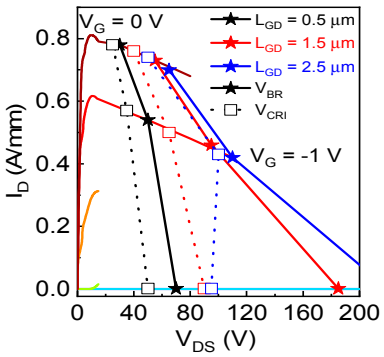

Fig. 9 V_{BR} comparison among devices with different L_{GD}.

D. Constant Voltage stress- off state

In order to evaluate the reliability of the devices under operating conditions, constant voltage stress tests in the off-state condition V_G = -5 V, V_D = 40 V were carried out. DC characteristics were measured at room temperature before, during (at each step) and after the stress.

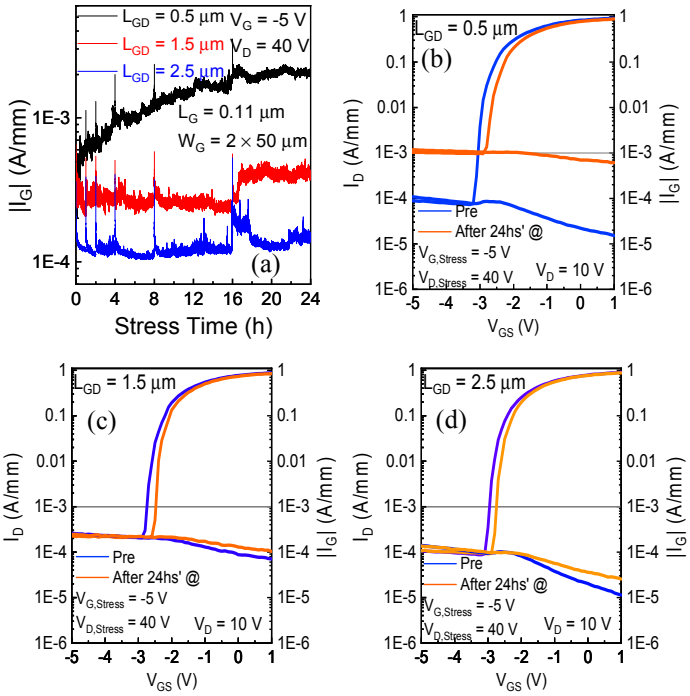

Fig. 10 (a) Drain current monitored during constant voltage stress, I_D-V_G curves during stress (b) 0.5 µm (c) 1.5 µm and (d) 2.5 µm devices.

Drain and gate leakage current during stress are shown in Fig. 10. Leakage current reached 1 mA/mm after four hours' stress for the device with 0.5 µm of L_{GD}, possibly due to the leakage path caused by trapping effects assisted by high electric field at the gate edge. The device with 1.5 µm and 2.5 µm of L_{GD} showed less than one order of magnitude increase in leakage current after 24 hours' stress.

The I_D-V_G curves of the devices at V_D = 10 V before and after 24 hours' stress are shown in Fig. 10(b)-(d). The L_{GD} = 0.5 µm devices showed one order of magnitude increase in leakage current, in accordance with the leakage current increase observed during stress. And the threshold voltage shifted positively by +0.3 V. The g_m-V_G curves in Fig. 11(a) showed that there is no $g_{m,max}$ decrease during stress.

For the devices with L_{GD} = 1.5 µm, there is almost no leakage current increase, similar to that observed during stress. The transfer characterization I_DV_G in Fig. 10(c) and g_m-V_G curves in Fig. 11 (b) showed that the degradation signature of the devices is V_{th} positive shift (+0.2 V). For the devices with L_{GD} = 2.5 µm, no leakage current increase or maximum transconductance increase is observed, similar to the device with L_{GD} = 1.5 µm, and the V_{TH} shift is close to +0.18 V.

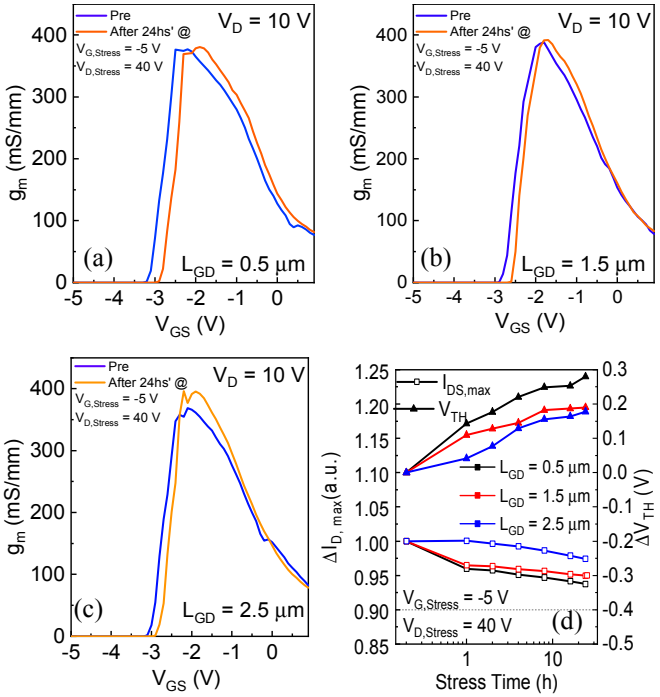

Fig. 11 Transfer g_m-V_G curves during stress of (a) 0.5 µm (b) 1.5 µm and (c) 2.5 µm devices and (d) I_{DSS} and V_{TH} shift during constant voltage stress at $V_{G,Stress}$ = -5 V, $V_{D,Stress}$ = 40 V.

The I_{DSS} decrease and V_{TH} shift during stress are summarized in Fig. 11 (d). The I_{DSS} decrease is less than 10%, and I_{DSS} degradation percentage and V_{TH} shift showed a dependence on L_{GD}.

IV. Discussions and Conclusions

From the results shown in the previous section, positive threshold voltage shift and leakage current increase has been observed during all the stress processes, regardless of bias voltage (off state, semi-on state and on state). Maximum transconductance decrease was observed at the step before breakdown during semi-on and on state stress, and the degradation percentage depends greatly on L_{GD}.

The V_{TH} shift during the off-state stress could be explained by the trapping effects under the gate, far from the device channel. In other words, when the device is cut-off, trapping effects in the G-D access region is difficult to happen. The traps could be generated in the GaN buffer far below the 2DEG [9], result from vacancy migration under high electric field [10], or owing to the heavy carbon doping in the GaN buffer [11].

Another explanation could be that during off state stress, electron tunneling occurs at the drain edge of the gate, and electrons are injected into the surface-state layer and captured by the surface deep donors, or charges at the SiN/AlN interface [12], hereby, the 2DEG density is decreased due to these negative surface charges, leading to V_{TH} positive shift [13].

At semi-on and on state, high current and high voltage exist at the same time during stress, making hot-electron effects [14]–[16] and self-heating effects[17] a an important factor during degradation. At the same time, the self-heating and hot electron effects will lead to inverse piezoelectric effect [18], and/or dehydration effects [19]. The hot electrons activated by high current stress could remove the hydrogen from pre-existing point defects (nitrogen antisite or Ga vacancy) and/or impurity complex, the dehydrogenation of the nitrogen antisite defect would lead to a decrease of the acceptor concentrations, leading to positive V_{TH} shift [20]. And the AlN/GaN lattice mismatch together with the high electric field will cause a critical strain in the devices, leading to mitigation of N, Al and/or Ga vacancies in AlN/GaN [10] and/or inverse piezoelectric effect [18].

In conclusion, short-term reliability and robustness of 110 nm AlN/GaN HEMTs has been evaluated by means off-state, semi-on state and on-state step stress tests and a constant voltage stress at off-state on devices having different gate-drain distance, L_{GD}. While breakdown voltages and critical voltages scale almost linearly with L_{GD}, failure mode remains almost unchanged in the nine device groups, and consists in an increase of gate leakage, accompanied by a positive shift of threshold voltage. In off-state, electroluminescence images detect the presence of localized leakage paths which may correspond to dislocations and act as preferential paths for electron trapping. Degradation is therefore preliminary attributed to trapping effects, enhanced by electric field, as shown in [21], [22]. In semi-on state and on-state, the effects of self-heating and trapping effects are the main cause of degradation.

ACKNOWLEDGEMENT

Support by EUGANIC project under the EDA Contract B 1447 IAP1 GP, by the EC Horizon 2020 ECSEL project 5G_GaN_2, and by the ESA ESTEC project RELGAN is gratefully acknowledged.

REFERENCES

[1] U. K. Mishra, P. Parikh, W. Yi-Feng, and Y. F. Wu, "AlGaN/GaN HEMTs-an overview of device operation and applications," *Proc. IEEE*, vol. 90, no. 6, pp. 1022–1031, 2002.

[2] G. H. Jessen *et al.*, "Short-channel effect limitations on high-frequency operation of AlGaN/ GaN HEMTs for T-gate devices," *IEEE Trans. Electron Devices*, vol. 54, no. 10, pp. 2589–2597, 2007.

[3] D. Marti, S. Tirelli, A. R. Alt, J. Roberts, and C. R. Bolognesi, "150-GHz cutoff frequencies and 2-W/mm output power at 40 GHz in a millimeter-wave AlGaN/GaN HEMT technology on silicon," *IEEE Electron Device Lett.*, vol. 33, no. 10, pp. 1372–1374, 2012.

[4] T. Zimmermann *et al.*, "AlN/GaN Insulated-Gate HEMTs With 2.3 A/mm Output Current and 480 mS/mm Transconductance," *Electron Device Lett. IEEE*, vol. 29, no. 7, pp. 661–664, 2008.

[5] K. Harrouche, R. Kabouche, E. Okada, and F. Medjdoub, "High Performance and Highly Robust AlN/GaN HEMTs for Millimeter-Wave Operation," *IEEE J. Electron Devices Soc.*, vol. 7, no. 1, pp. 1145–1150, 2019.

[6] G. Meneghesso *et al.*, "First Reliability Demonstration of Sub-200-nm AlN/GaN-on-Silicon Double-Heterostructure HEMTs for Ka-Band Applications," *IEEE Trans. Device Mater. Reliab.*, vol. 13, no. 4, pp. 480–488, Dec. 2013.

[7] T. Kemmer *et al.*, "Voltage- and Temperature-Dependent Degradation of AIN/GaN High Electron Mobility Transistors," in *2018 International Integrated Reliability Workshop (IIRW)*, 2018, vol. 2018-Octob, pp. 1–6.

[8] M. Rzin *et al.*, "Linearity and robustness evaluation of 150-nm AlN/GaN HEMTs," *Microelectron. Reliab.*, vol. 100–101, no. June, p. 113388, Sep. 2019.

[9] Z. Zhang *et al.*, "Correlation of proton irradiation induced threshold voltage shifts to deep level traps in AlGaN/GaN heterostructures," *J. Appl. Phys.*, vol. 119, no. 16, pp. 2–8, Apr. 2016.

[10] K. H. Warnick, Y. Puzyrev, T. Roy, D. M. Fleetwood, R. D. Schrimpf, and S. T. Pantelides, "Room-temperature diffusive phenomena in semiconductors: The case of AlGaN," *Phys. Rev. B*, vol. 84, no. 21, p. 214109, Dec. 2011.

[11] A. Chini *et al.*, "Experimental and Numerical Analysis of Hole Emission Process from Carbon-Related Traps in GaN Buffer Layers," *IEEE Trans. Electron Devices*, vol. 63, no. 9, pp. 3473–3478, 2016.

[12] M. Meneghini *et al.*, "Negative Bias-Induced Threshold Voltage Instability in GaN-on-Si Power HEMTs," *IEEE Electron Device Lett.*, vol. 37, no. 4, pp. 474–477, Apr. 2016.

[13] M. Faqir, G. Verzellesi, G. Meneghesso, E. Zanoni, and F. Fantini, "Investigation of high-electric-field degradation effects in AlGaN/GaN HEMTs," *IEEE Trans. Electron Devices*, vol. 55, no. 7, pp. 1592–1602, 2008.

[14] S. T. Pantelides *et al.*, "Reliability of III–V devices – The defects that cause the trouble," *Microelectron. Eng.*, vol. 90, pp. 3–8, Feb. 2012.

[15] R. Jiang *et al.*, "Degradation and annealing effects caused by oxygen in AlGaN/GaN high electron mobility transistors," *Appl. Phys. Lett.*, vol. 109, no. 2, 2016.

[16] T. Brazzini *et al.*, "Hot-Electron Electroluminescence under RF Operation in GaN-HEMTs: A Comparison among Operational Classes," *IEEE Trans. Electron Devices*, vol. 64, no. 5, pp. 2155–2160, 2017.

[17] X. D. Wang, W. Da Hu, X. S. Chen, and W. Lu, "The study of self-heating and hot-electron effects for AlGaN/GaN double-channel HEMTs," *IEEE Trans. Electron Devices*, vol. 59, no. 5, pp. 1393–1401, 2012.

[18] Jungwoo Joh and J. A. del Alamo, "Critical Voltage for Electrical Degradation of GaN High-Electron Mobility Transistors," *IEEE Electron Device Lett.*, vol. 29, no. 4, pp. 287–289, Apr. 2008.

[19] Y. S. Puzyrev *et al.*, "Dehydrogenation of defects and hot-electron degradation in GaN high-electron-mobility transistors," *J. Appl. Phys.*, vol. 109, no. 3, 2011.

[20] T. Roy *et al.*, "Electrical-stress-induced degradation in AlGaN/GaN high electron mobility transistors grown under gallium-rich, nitrogen-rich, and ammonia-rich conditions," *Appl. Phys. Lett.*, vol. 96, no. 13, 2010.
[21] R. Jiang *et al.*, "Multiple Defects Cause Degradation After High Field Stress in AlGaN/GaN HEMTs," *IEEE Trans. Device Mater. Reliab.*, vol. 18, no. 3, pp. 364–376, Sep. 2018.
[22] J. Bergsten *et al.*, "Electron Trapping in Extended Defects in Microwave AlGaN/GaN HEMTs with Carbon-Doped Buffers," *IEEE Trans. Electron Devices*, vol. 65, no. 6, pp. 2446–2453, 2018.